Genomic Insights into a Multispecies Bacterial Pathogen Complex Driving Bacterial Blotch in White Button Mushrooms.

Sameerika D Mudiyanselage[1], Michelle Lee[1], Jose C. Huguet-Tapia[1], Romina Gazis[2*], Samuel J Martins[1*].

[1]Department of Plant Pathology, University of Florida, Gainesville, FL, 32611, USA.

[2]Department of Plant Pathology, Tropical Research Education Center, Homestead. FL, 33031-3314, USA.

*Correspondence:

Samuel J Martins

Romina Gazis

Email: sj.martins@ufl.edu

Author Contributions: S.J.M. obtained the funding source; S.D.M., S.J.M., and R.G. designed the research; S.D.M. performed experiments; S.J.M. and M.L. assisted with experimental work; J.H. contributed to bioinformatics analyses; S.D.M. wrote the manuscript; R.G., and S.J.M reviewed the manuscript.

Competing Interest Statement: The authors declare no competing interests.

Classification: Biological Science

Keywords: *Agaricus bisporus*, *Pseudomonas azotoformans*, Multilocus sequence alignment, Average nucleotide identity, Whole genome sequencing.

This PDF file includes: Main Text
Figures 1 to 5
Tables 1

ABSTRACT

Bacterial blotch remains a major constraint to global white button mushroom (*Agaricus bisporus*) production, yet its etiological complexity has been underestimated. Through a genome-resolved, polyphasic approach applied to symptomatic mushrooms from two U.S. farms, we uncovered an unexpectedly diverse complex of *Pseudomonas* species driving blotch disease. Beyond classical pathogens (*P. tolaasii*, *P. gingeri*, *P. agarici*, and *P.* "*reactans*", *P. yamanorum*, *Pseudomonas* sp. NC02), our analyses revealed a striking prevalence of *P. azotoformans*, a species not previously associated with mushroom pathology, alongside *P. pergaminensis*, *P. monsensis*, *P. tensinigenes*, *P. simiae*, *Pseudomonas* sp. Irchel 3A7, *Pseudomonas* sp. REP124 and two putatively novel lineages. Comparative genomics demonstrated pronounced heterogeneity in accessory genome content, with *P. azotoformans* exhibiting exceptional genomic plasticity indicative of broad ecological adaptability. Secondary metabolite profiling and white-line assays further delineated species-specific chemotaxonomic signatures, underscoring the multifactorial nature of virulence. Collectively, this study provides the most comprehensive genomic and phenotypic characterization of blotch-associated *Pseudomonas* to date, overturning the long-held paradigm of a single dominant pathogen. By establishing that bacterial blotch is a regionally structured, multispecies disease complex, our findings redefine its epidemiology and lay the foundation for improved diagnostics, surveillance, and integrated management strategies in mushroom production systems.

SIGNIFICANCE STATEMENT

Bacterial blotch disease has long been attributed to a narrow set of *Pseudomonas* species, shaping decades of diagnostic and management practices in mushroom production. Our study overturns this paradigm by revealing that blotch is caused by a highly diverse, regionally structured pathogen complex *Pseudomonas* species, including multiple species never before linked to mushrooms. Using a genome-resolved, polyphasic framework, we demonstrated that accessory genome expansion and secondary metabolite diversity collectively drive pathogenic variability. The unexpected dominance of *Pseudomonas azotoformans*, a species previously known only from plant and environmental contexts,

signals an emerging threat with broad ecological implications. These findings redefine the epidemiology of blotch disease, establish a new foundation for genomic surveillance, and highlight the urgent need for integrated management strategies that account for multispecies pathogen dynamics. By bridging microbial ecology, comparative genomics, and applied plant pathology, this work provides actionable insights for improving food security and sustainability in one of the world's most economically important specialty crops.

INTRODUCTION

The white button mushroom (*A. bisporus*) is one of the fastest growing and most widely cultivated mushroom species globally, with major production hubs in China, the United States, the Netherlands, Poland, Italy, and India. In the United States alone, white button mushrooms represent over 90% of total mushroom consumption underscoring their central role in the national and global mushroom markets (1). However, despite their economic importance, the industry faces a significant and persistent threat from "bacterial blotch", one of the most destructive postharvest diseases affecting *A. bisporus,* which has impacted commercial production worldwide for decades (2, 3).

Bacterial blotch is primarily associated with *Pseudomonas* species, metabolically versatile and ubiquitous bacteria that naturally inhabit the casing layer. Some *Pseudomonas* strains, such as *P. putida* (4) and *P. poae* n12 (5), play beneficial roles in mushroom cultivation promoting *A. bisporus* growth and contributing to primordia formation. However, pathogenic *Pseudomonas* species often persist in casing materials even after pasteurization, leading to disease outbreaks. The bacterial blotch disease is characterized by rapid discoloration of the mushroom cap, pitting, tissue degradation, and, ultimately, extensive postharvest losses. Different blotch phenotypes correspond to different pathogens: *P. tolaasii* causes brown blotch, producing sunken greenish-brown lesions that expand and coalesce (3), while *P. gingeri* causes ginger blotch, marked by golden-yellow discoloration (6). Beyond these well-known species, few surveys have revealed a much broader diversity of blotch-causing bacteria, including *P. agarici* (7–9), *P.* "*reactans*" (10), *Pseudomonas* sp. NZ17*P* (11)*, P costantinii* (12, 13), *P. yamanorum*, *P. edaphica*, *P. salomonii*,

Pseudomonas sp. NC02 (12), and *P. extremorientalis* (14). A few non-*Pseudomonas* species have been reported in the years to cause blotch-like symptoms, which include *Mycetocola* sp. (15), *Serratia liquefaciens*, *S. proteamaculans*, *Pantoea* sp. (12), and *Cedecea neteri* (16), highlighting the increasing complexity of this disease.

Pathogenic *Pseudomonas* species employ multiple virulence mechanisms, including extracellular proteases and lipases (17), antifungal metabolites (18), and cyclic lipopeptides (CLPs) that enhance motility, surface colonization, competition, and infection. In addition to pathogen-derived factors, the development of blotch symptoms is influenced by the mushroom's physiological responses, particularly enhanced tyrosinase activity and increased phenolic content, which collectively accelerate browning and tissue discoloration (3).

Historically, the identification of bacterial blotch-causing *Pseudomonas* species has relied heavily on phenotypic assays such as the White Line Agar Assay (WLA), which detects the interaction between tolaasin produced by *P. tolaasii* and the WLIP compound produced by the organism described as *P. reactans*. However, the increasing diversity of blotch-causing *Pseudomonas* species and the frequent inconsistency of WLA results have made it clear that phenotypic tests alone are insufficient for accurate species identification. Although multilocus sequence analysis (MLSA) and 16S rRNA-based approaches have been widely used for *Pseudomonas* taxonomy, several studies have demonstrated their limitations, particularly in resolving closely related taxa (19). Consequently, modern polyphasic strategies that combine MLSA, whole-genome comparisons, and chemotaxonomic profiling now provide the most robust framework for species-level resolution within the genus *Pseudomonas*.

Despite decades of research, the complete and accurate diversity of blotch-causing *Pseudomonas* species remains unresolved, highlighting the urgent need for broader surveys that address both identification and management, as effective control strategies depend on precise pathogen recognition. This growing complexity underscores the importance of region-specific assessments of pathogen diversity. In this study, we conducted a systematic survey of symptomatic white button mushrooms collected from two commercial production sites in the United States. Specifically, we aimed to characterize the causative

agents of bacterial blotch by integrating phenotypic assays (WLA and fluorescence), pathogenicity tests, MLSA, whole-genome analyses, comparative genomics, and *in silico* profiling of secondary metabolite biosynthetic gene clusters. Together, these approaches provided a comprehensive overview of the bacterial blotch pathogens present in these production systems and their associated dynamics on *Agaricus bisporus.*

RESULTS

Isolation of *Pseudomonas* spp. from white button mushrooms

During the mushroom survey, we collected 28 symptomatic white button mushrooms from Farm X and 17 from farm Y located in two states in the U.S., both exhibiting typical bacterial blotch symptoms. The symptoms varied in severity, ranging from light yellow, known as "ginger blotch", to dark brown or chocolate-colored lesions referred to as "brown blotch". These symptoms were often accompanied by sunken, water-soaked areas and collapse of the wet tissue (Fig. 1A). A total of 76 bacterial isolates were selectively recovered from the samples using NCP-KB medium and were used for subsequent analyses.

To identify isogenic strains prior to further genomic and phenotypic characterization, BOX-PCR fingerprinting was performed on the 76 bacterial isolates recovered from the symptomatic mushrooms. The BOX-PCR profiles exhibited banding patterns in agarose gel ranging from <0.5 kb to approximately 10 kb. A binary data matrix representing the presence or absence of 23 distinct BOX-PCR bands was generated and subjected to clustering analysis. The resulting dendrogram (*SI Appendix*) revealed 60 isolate groups at a 90% similarity threshold, representing 76 distinct isolates with varying degrees of relatedness. This clustering pattern demonstrated a high level of genetic diversity among the isolates while also identifying 10 groups of closely related strains (isolate group 8, 14, 18, 23, 26, 37, 39, 40, 57, and 58). Based on these DNA fingerprint patterns, 15 isolates exhibiting identical BOX-PCR profiles were considered isogenic and excluded from subsequent analyses.

121 **Pathogenicity Assay**

122 The ability of each isolate to cause bacterial blotch symptoms was assessed *in vitro* by
123 inoculating fresh mushroom tissue cubes with each of the 61 selected isolates from the
124 BOX-PCR profiles. In this study, pathogenicity was defined as the ability to induce
125 discoloration on mushroom tissue within 2 days post-inoculation, in contrast to the
126 controls. A total of 85% of the strains were identified as producing extensive discoloration
127 accompanied by tissue pitting. An additional 7% of isolates produced only rapid tissue
128 discoloration without tissue pitting, while 8% exhibited only mild or slow discoloration,
129 comparable to the nonpathogenic control strains *Pseudomonas protegens* BP1304 and
130 *Pseudomonas tolaasii* BP1106 within 48 h post-inoculation (Table 1).

131

132 **Evaluating the potential for lipopeptide and fluorescent pigment production**

133 Among the 61 bacterial isolates examined, eight produced a white-line reaction when
134 confronted with *Pseudomonas fluorescens* Pf5, indicating the presence of tolaasin-like
135 lipopeptides typically associated with *P. tolaasii* or closely related species. In contrast,
136 twenty-four isolates formed a distinct white line when challenged with *P. tolaasii* BP1106,
137 consistent with the production of WLIP or WLIP-like noncanonical lipopeptides. The
138 remaining 29 isolates showed no reaction with either *P. fluorescens* Pf5 or *P. tolaasii*
139 BP1106 (Table 1, Fig. 1B). Nearly all isolates exhibited fluorescence under UV
140 illumination (365 nm), indicative of pyoverdine production, except for two isolates
141 (SM395 and SM405), which did not fluoresce (Table 1).

142

143

144

145

146

147

148

149

150

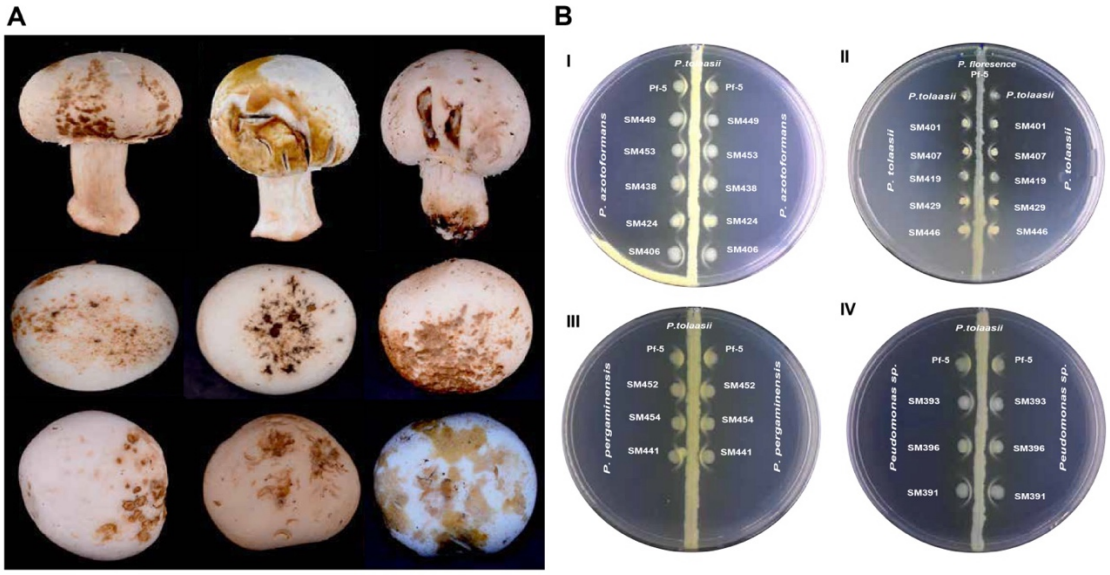

Fig. 1. ***Phenotypic characterization of bacterial blotch pathogens from white button mushroom collected at two U.S. farms (X and Y) in the U.S.*** *(A) Representative blotch symptoms on mushroom caps, ranging from brown to ginger discoloration with varying degrees of tissue pitting. (B) White-line reaction assays illustrating lipopeptide-mediated interactions among Pseudomonas isolates: B(I) P. azotoformans versus P. tolaasii BP1106; B(II) P. tolaasii isolates versus P. fluorescens Pf-5; B(III) P. pergaminensis isolates versus P. tolaasii BP1106; B(IV) isolates SM391, SM393, and SM396 versus P. tolaasii BP1106. Distinct white precipitate lines indicate positive interactions characteristic of cyclic lipopeptide production.*

Table 1. *Phenotypic characterization of isolates based on pathogenicity, white-line agar Assay (WLA), and fluorescence production.*

Isolates	Pathogenicity Score*	White Line Agar Assay (WLA)†		Florescence under UV‡
		P. fluorescens Pf5	*P. tolaasii BP1106*	
SM405	1	0	0	N
SM432	3	0	0	Y
SM395	1	0	0	N
SM445	3	0	1	Y
SM434	3	0	0	Y
SM421	3	0	0	Y
SM402	3	0	1	Y
SM453	3	0	1	Y
SM439	3	0	0	Y
SM416	3	0	0	Y
SM451	3	0	1	Y
SM411	3	0	0	Y
SM438	3	0	1	Y
SM433	3	0	0	Y
SM410	3	0	0	Y
SM399	3	0	0	Y
SM428	3	0	0	Y
SM396	3	0	1	Y
SM408	3	0	1	Y

SM442	3	0	0	Y
SM436	3	0	1	Y
SM424	3	0	1	Y
SM392	3	0	0	Y
SM448	1	0	0	Y
SM449	3	0	1	Y
SM417	2	0	0	Y
SM391	3	0	1	Y
SM400	1	0	0	Y
SM393	3	0	1	Y
SM444	3	0	1	Y
SM401	3	1	0	Y
SM403	3	1	0	Y
SM409	3	0	0	Y
SM431	3	0	0	Y
SM423	3	0	1	Y
SM404	3	0	0	Y
SM406	3	0	1	Y
SM390	3	0	0	Y
SM397	3	0	0	Y
SM446	3	1	0	Y
SM437	3	1	0	Y
SM450	3	0	1	Y
SM419	3	1	0	Y
SM407	3	1	0	Y
SM441	3	0	1	Y
SM418	3	0	1	Y
SM394	3	0	1	Y
SM429	3	1	0	Y
SM454	3	0	1	Y
SM398	3	0	1	Y
SM452	3	0	1	Y
SM413	3	0	1	Y
SM447	2	0	1	Y
SM420	3	0	0	Y
SM415	2	0	0	Y
SM425	3	0	0	Y
SM426	1	0	0	Y
SM440	3	0	0	Y
SM422	3	0	0	Y
SM412	3	0	0	Y
SM430	2	1	0	Y

*Pathogenicity Score, 1= mild or slow discoloration; 2= rapid tissue discoloration without tissue pitting; 3= extensive discoloration accompanied by tissue pitting.
†White line Agar Assay, 1= presence; 0= White line absence
‡Florescence under UV, Y= Florescence; N= non-florescence

Whole genome sequencing of *Pseudomonas* isolates

We analyzed the whole genomes of 57 pathogenic *Pseudomonas* strains isolated from *Agaricus bisporus*. Illumina paired-end sequencing produced an average of 1.77 million read pairs per genome, with a range of 1.0 to 3.4 million. Over 95% of bases exceeded a Phred quality score of Q30. De novo assemblies yielded an average of 185 contigs per genome, with a mean total length of 6.77 Mb, N50 values averaging 96,095 bp, and a GC content of 61%. BUSCO analysis indicated an average genome completeness of 98%, with no detected genome duplication, fragmentation, or missing regions, ensuring high-quality data suitable for genome assembly and downstream analyses. Dataset S02 provides summary statistics of the assembly.

191

192 **Genome-wide comparison and Taxonomic classification**

193 To ensure accurate taxonomic classification and avoid potential misidentifications
194 associated with conventional methods, we employed a polyphasic approach that integrates
195 several complementary analyses. The *Pseudomonas* isolates were first evaluated using the
196 Genome Taxonomy Database Toolkit (GTDB-Tk) and the Type Strain Genome Server
197 (TYGS) for whole-genome-based taxonomic assignment. Additionally, we performed
198 multilocus sequence analysis (MLSA) of 8 conserved housekeeping genes and FastANI-
199 based average nucleotide identity comparisons to confirm species-level classifications.
200 This integrated approach provided a highly reliable and comprehensive strategy for
201 resolving taxonomic relationships within the *Pseudomonas* genus.

202 We initially used GTDB-Tk for whole-genome classification, relying on GTDB-Tk-based
203 ANI measurements to achieve high-resolution species-level assignments of the isolates.
204 We identified *Pseudomonas "gingeri*" (*n* = 11), *P. azotoformans* (*n* = 10), *P. tolaasii* (*n* =
205 7), *P. pergaminensis* (*n* = 6), and *Pseudomonas "reactans"* (*n* = 2), as well as single
206 isolates of *P. agarici, P. simiae, P. monsensis, P. yamanorum*, and *P. tensinigenes*. A
207 species boundary of >95% ANI and <83% for interspecies divergence was adopted. Isolate
208 SM400 shared 94% GTDB-Tk-based ANI with *P. allokribbensis*, while SM426 exhibited
209 90% ANI with *P. azerbaijanoccidens*, indicating low relatedness. In total, 14 isolates could
210 not be confidently assigned to any *Pseudomonas* species and were not further explored in
211 this study that focused on *Pseudomonas* species. Among these, SM412, SM422, SM425,
212 and SM440 showed >95% ANI to *Pseudomonas* sp. NC02, while SM415 and SM430
213 showed >95% to *Pseudomonas* sp. Irchel 3A7 and *Pseudomonas* sp. REP124, respectively.
214 The remaining isolates SM390, SM391, SM393, SM396, SM397, SM404, SM409, and
215 SM431 did not show >95% ANI to any species represented in the GTDB-Tk database,
216 indicating that they may represent previously uncharacterized *Pseudomonas* lineages.

217 We further characterized the isolates using the TYGS, which utilizes a curated database of
218 prokaryotic type strains for whole-genome-based taxonomic classification. This analysis
219 identified isolates belonging to *P. tolaasii, P. pergaminensis, P. agarici, P. simiae, P.*
220 *monsensis,* and *P. yamanorum*, with digital DNA-DNA hybridization (dDDH) values

221 exceeding the 70% species delineation threshold (30), consistent with the results obtained
222 from GTDB-TK classification. In contrast, the *P. tensinigenes* isolate showed a slightly
223 lower dDDH value (66%). However, due to the absence of corresponding valid type strains
224 in the TYGS database, *Pseudomonas "gingeri"*, *Pseudomonas* "*reactans*", and *P.*
225 *azotoformans* could not be validated. Additionally, the remaining 14 *Pseudomonas* isolates
226 could not be resolved to any known type strain in the database. The complete list of ANI
227 and dDDH values for all isolates is provided in Dataset S01.
228 To assess genetic relatedness among mushroom-associated *Pseudomonas* isolates, we
229 conducted pairwise Average Nucleotide Identity (ANI) analyses. Using a ≥ 95% ANI
230 threshold for species delineation, the dataset resolved into 14 distinct genomic clusters,
231 capturing the full spectrum of intra and interspecific diversity within the collection (Fig.
232 2A). Comparative analyses with closely related reference type strains enabled the
233 assignment of multiple clusters to recognize species, including *P. "gingeri", P.*
234 *azotoformans, P. tolaasii, P. pergaminensis, P. "reactans", P. agarici, P. simiae, P.*
235 *monsensis, P. yamanorum*, and *P. tensinigenes*, with clustering patterns aligning with
236 taxonomic classifications derived from TYGS and GTDB analyses. Isolates SM400 and
237 SM426 did not cluster with *P. allokribbensis* and *P. azerbaijanoccidens*, respectively,
238 indicating significant genomic divergence from these reference strains. The remaining 14
239 isolates formed three distinct genomic clusters: Cluster 1 (SM412, SM422, SM425,
240 SM440), Cluster 2 (SM391, SM393, SM396), and Cluster 3 (SM390, SM397, SM404,
241 SM409, SM431), with SM415 and SM430 representing distinct lineages.
242
243 **Multi-locus sequence analysis (MLSA)**
244 To evaluate the commonly used MLSA for taxonomic resolution and compare it with
245 phylogenomic inference, we selected eight conserved housekeeping genes *rpoD, rpoB,*
246 *recA, gapA, gltA, atpD, gyrB*, and *ileS* as molecular barcodes based on their established
247 discriminatory power and phylogenetic stability (19). A maximum-likelihood phylogeny
248 was reconstructed from the concatenated sequences of these loci for 57 *Pseudomonas*
249 isolates, including 32 type strains.

The largest lineage corresponded to *Pseudomonas* "*gingeri*", comprising 11 isolates. Three major sister clades were resolved, including an independent lineage represented by SM434, while the remaining reference strains formed a separate, well-supported subclade. SM416 grouped with the type strain *P. agarici* LMG 2112^{T}, forming a distinct and clearly separated lineage. Consistent with ANI and GTDB-Tk assignments, seven isolates clustered with *P. tolaasii* NCPPB 2192^{T}, while six isolates grouped with *P. pergaminensis* 1008^{T} and Z7.15^{T}. Similarly, ten isolates clustered with *P. azotoformans* S4^{T}, and SM423 and SM450 grouped with *P*. "*reactans*" C5002. Several isolates exhibited broader genomic affinities, with *P. monsensis*, *P. tensinigenes*, *P. allokribbensis,* and *P. azerbaijanoccida* forming closely related yet distinct branches. Furthermore, SM415 and SM430 resolved into two independent lineages. Additional well-supported isolate clusters included SM412, SM422, SM425, SM440; SM391, SM393, SM396; and SM390, SM397, SM404, SM409, and SM431.

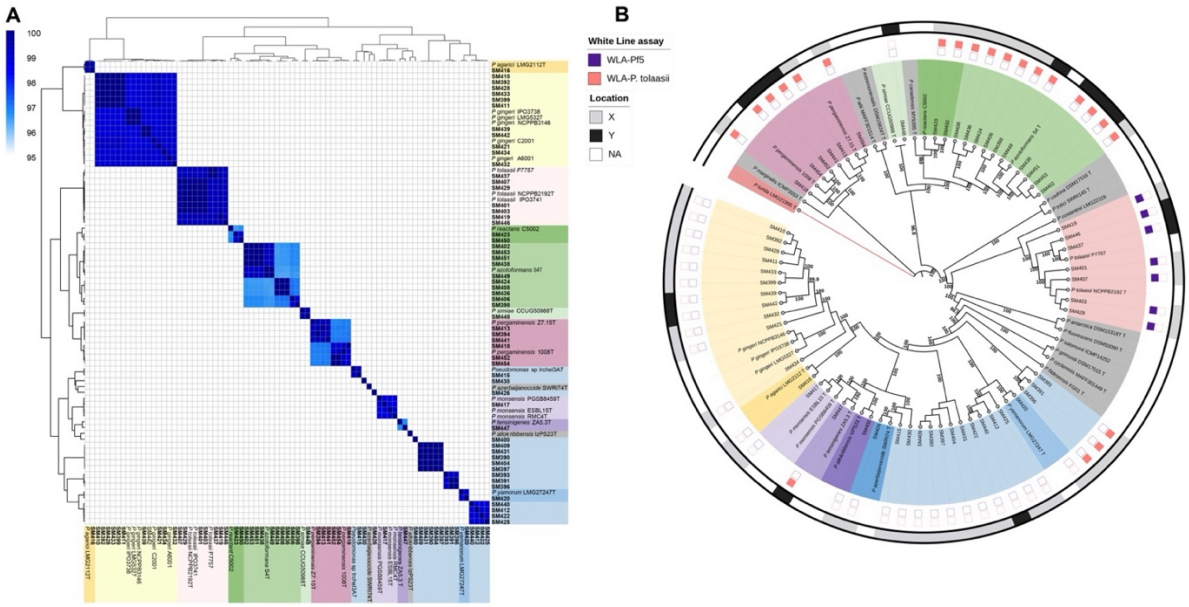

Fig. 2. *Genomic taxonomy and phylogenetic relationships of Pseudomonas isolates associated with bacterial blotch in white button mushrooms (Agaricus bisporus) from two U.S. farms (X and Y).* *(A) Heatmap of pairwise whole-genome Average Nucleotide Identity (ANI) among 57 blotch-associated isolates and 22 reference strains. Color intensity reflects genome similarity, with values ≥95% indicating species-level identity. Axis labels are color-coded by species cluster. (B) Circular maximum-likelihood*

phylogenetic tree reconstructed from concatenated sequences of nine housekeeping genes (rpoD, rpoB, recA, gapA, gltA, atpD, gyrB, and ileS) for 57 isolates and 31 reference strains. Bootstrap support values ≥95% are shown; branch lengths are not to scale. Pseudomonas lurida served as the outgroup. The outer ring denotes farm origin (X or Y), while inner markers indicate white-line assay results: pink squares = positive interaction with P. tolaasii BP1106; purple squares = positive interaction with P. fluorescens Pf-5.

Comparative Pan-Genome Analysis

Roary identified 1,206 core genes and 45,131 accessory genes across the 57 *Pseudomonas* isolates. Among these, 133 soft-core genes were present in at least 95% but fewer than 99% of strains; 9,240 shell genes were present in at least 15% but fewer than 95% of strains; and 35,758 cloud genes were present in at least one strain but fewer than 15%. In total, the pangenome comprised 46,337 genes, highlighting extensive genomic diversity among the isolates. We analyzed the core and pangenome of the four dominant *Pseudomonas* species: *P. tolaasii, P. pergaminensis, P. "gingeri"*, and *P. azotoformans* (Fig. 3). In *P. tolaasii*, the pangenome comprised 8,356 genes, including 5,161 core genes (62%) shared across nearly all isolates, and an accessory genome of 3,195 genes (1,118 shell and 2,077 cloud). *P. pergaminensis* showed a comparable pattern, with a total of 9,092 genes, of which 4,745 (52%) were core; the accessory genome consisted of 2,339 shell and 2,008 cloud genes. *P.* "*gingeri*" harbored 9,026 total genes, including 5,560 core genes (62%) and an accessory component of 1,842 shell and 1,624 cloud genes. These species displayed consistently high core-to-pan-genome ratios, indicating that most isolates share a conserved set of essential metabolic and structural functions.

In contrast, *P. azotoformans* exhibited a markedly expansive pan-genome, with 18,029 genes but only 2,477 core genes (14%). Its accessory genome was dominated by 6,858 shell and 8,694 cloud genes, reflecting extensive genomic variability and a substantially more flexible gene repertoire.

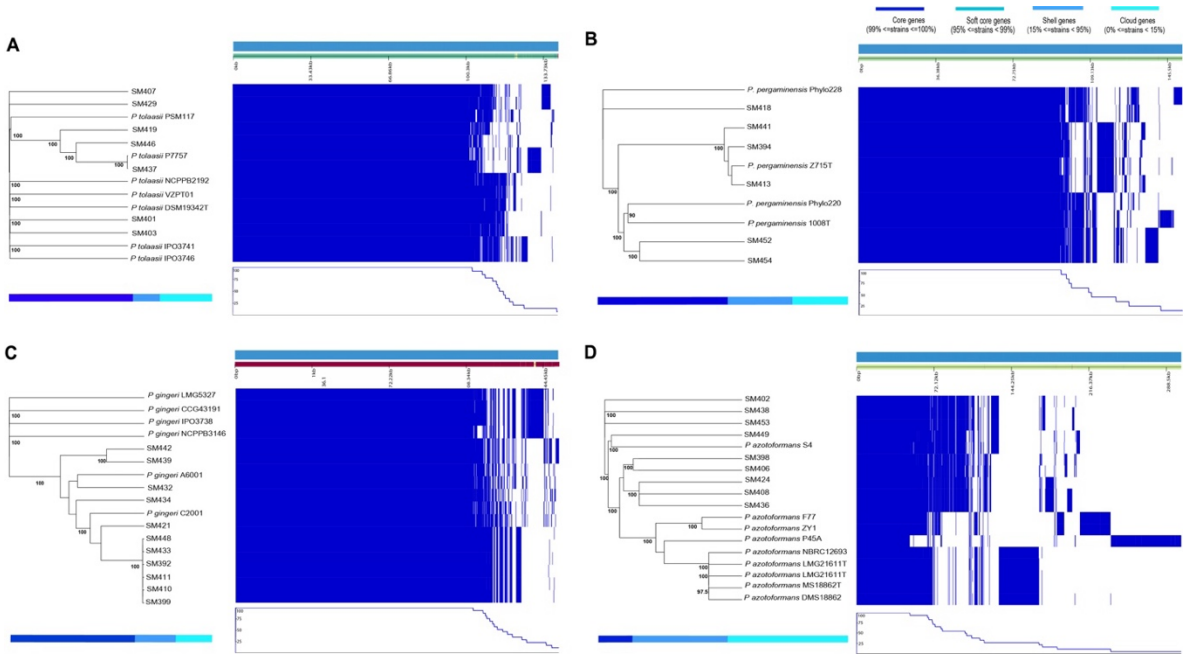

Fig. 3. ***Core and pangenome architecture of four Pseudomonas species associated with bacterial blotch in white button mushrooms (Agaricus bisporus) from two U.S. farms (X and Y).*** *(A) P. tolaasii; (B) P. pergaminensis; (C) Pseudomonas "gingeri"; (D) P. azotoformans. Each panel shows a maximum-likelihood phylogenetic tree based on core gene alignments for the respective species cluster, alongside a gene presence–absence matrix. Rows correspond to individual genomes; columns represent orthologous gene families. Blue blocks indicate gene presence; white blocks indicate absence. Bar graphs summarize the proportion of core, soft-core, shell, and cloud genes, illustrating species-specific genomic diversity and accessory genome expansion.*

Diversity and distribution of biosynthetic gene clusters among *Pseudomonas* isolates

Beyond DNA-based taxonomy, we generated *in silico* secondary metabolite profiles to examine chemotaxonomic patterns among blotch-associated *Pseudomonas* species. Genome mining of the 57 *Pseudomonas* isolates using antiSMASH revealed a substantial biosynthetic diversity, encompassing 22 distinct families of secondary metabolite biosynthetic gene clusters (BGC) (Fig. 4). The presence-absence matrix illustrates the

distribution of major BGC classes, including numerous nonribosomal peptide synthetase (NRPS) loci encoding cyclic lipopeptides such as tolaasin, viscosin, ririwpeptide, lokisin, syringafactin, putisolvin, orfamides B, syringocin, histicorrugatin, necroxime, stechlisin, sessilin, bananamide, and corpeptin-like families. Siderophore-associated clusters were abundant and phylogenetically widespread, including EDHA, yersiniabactin, Ni-siderophore, enantio-pyochelin, and azotobactin D. Several isolates also encoded BGCs for volatile or antibiotic metabolites such as sodorifen, geosmin, and 2,4-diacetylphloroglucinol. Distinct chemotaxonomic signatures emerged across species: *P. gingeri* encoded volatile and antibiotic loci; *P. pergaminensis* consistently carried viscosin; *P. tolaasii* harbored tolaasin; and viscosin clusters were widely distributed across several lineages, including *P. "reactans"*. Cluster-specific patterns were evident, with Cluster 1 enriched in enantio-pyochelin and Cluster 3 encoding combinations of tolaasin and riripeptide like loci. Notably, *P. azotoformans* lacked known BGCs for CLPs, siderophores, volatiles, or antibiotics, suggesting unexplored or cryptic metabolic pathways.

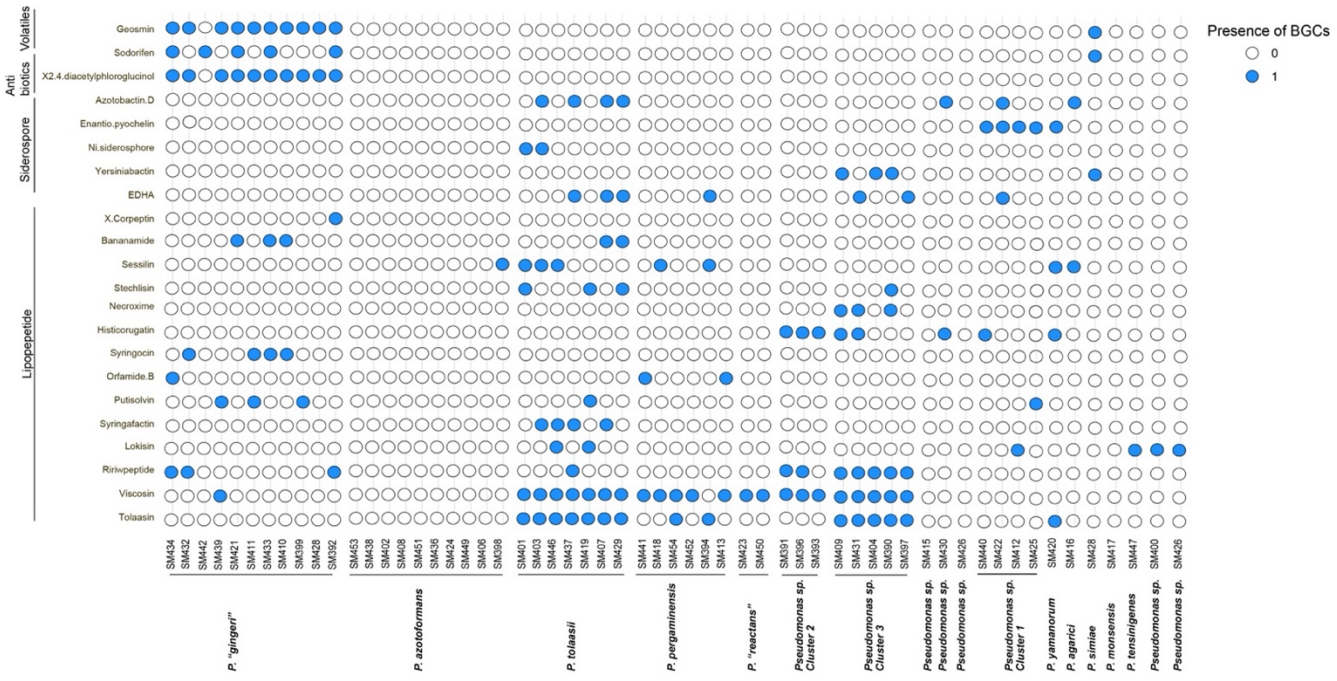

Fig. 4. ***Distribution of 22 Biosynthetic gene cluster (BGC) families across 57 Pseudomonas isolates***. *Columns represent individual isolates; rows correspond to BGC*

families grouped into four functional categories: lipopeptides, siderophores, antibiotics, and volatiles. Blue dots indicate predicted presence of a BGC family as identified by antiSMASH; white dots indicate absence.

Pathogenicity assessment

To assess the range of symptom patterns we monitored disease progression over a 48-hour period after inoculation. In Fig. 5 we summarized the symptoms induced by individual *Pseudomonas* species on mushroom cap tissues. Apart from the characteristic "brown blotch" and "ginger blotch" symptoms caused by *P. tolaasii* and *Pseudomonas* "gingeri," respectively, the additional species identified in this study produced distinct lesion phenotypes. For instance, *P. pergaminensis* induced lighter brown lesions accompanied by pronounced tissue pitting, whereas *P. yamanorum* generated pale yellow discoloration, also associated with noticeable pitting. In contrast, isolates belonging to Cluster 3 were mainly associated with dark, chocolate-brown discoloration and fine, needle-like pitting as the infection progressed. Isolates from Cluster 1 produced pale brown lesions with limited pitting but evident tissue damage. *P. azotoformans* caused irregular brown blotches with slight pitting progression, while *P. agarici* produced wet, yellowish tissue with little or no pitting. *P. monsensis* and *P. tensinigenes* both exhibited dark black discoloration without significant tissue damage or pitting. Furthermore, *P. simiae,* isolates in Cluster 2, SM400, and SM426 caused only slight discoloration compared to the nonpathogenic control.

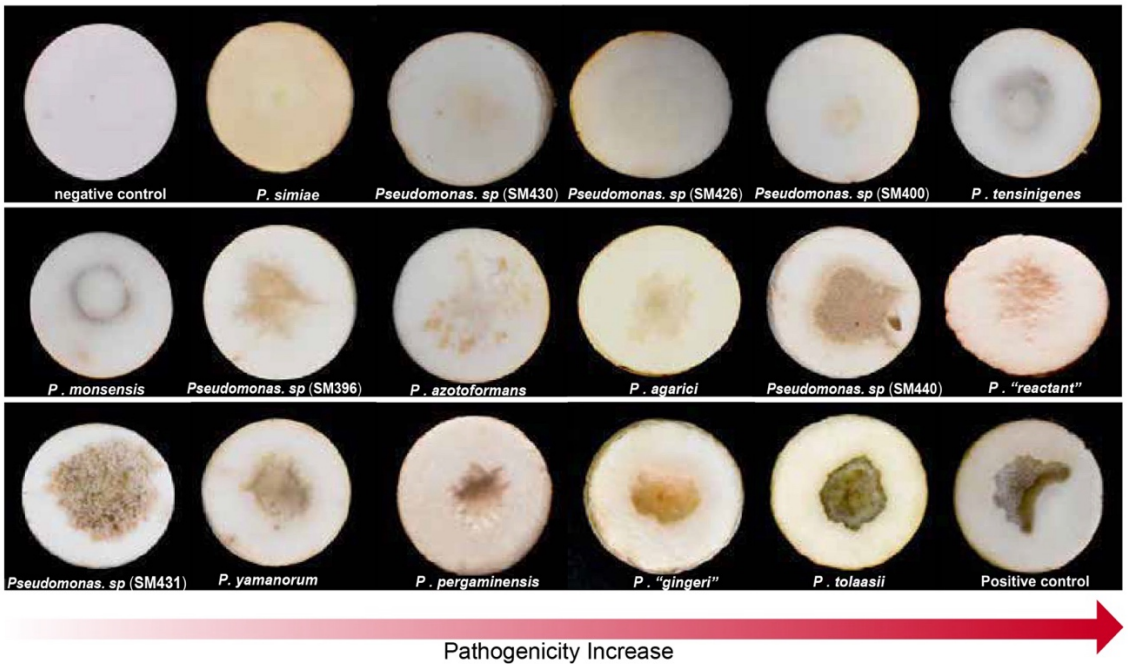

401 **Fig. 5.** ***Pathogenicity assays of representative Pseudomonas species clusters inoculated***
402 ***on fresh white button mushroom tissue****. Lesion phenotypes range from extensive*
403 *discoloration with pronounced tissue pitting to rapid surface browning and mild or slow*
404 *discoloration. Arrows indicate increasing pathogenic severity across species clusters*.
405

406 **Discussion**

407 In this study, we isolated and characterized bacterial blotch-causing *Pseudomonas* from
408 white button mushrooms collected from two southern states in the USA. Among the 56
409 isolates, we identified well-known blotch pathogens, including *Pseudomonas "gingeri*"
410 (*n* = 11), *P. tolaasii* (*n* = 7), *Pseudomonas* sp. NC02 (*n* = 4), and *Pseudomonas "reactans"*
411 (*n* = 2), along with single isolates of *P. yamanorum*, and *P. agarici*. Additionally, we
412 identified seven bacterial taxa that had not been previously reported as associated with
413 blotch disease, including *P. azotoformans* (*n* = 10), *P. pergaminensis* (*n* = 6)*, P. monsensis*,
414 *P. tensinigenes*, *P. simiae*, *Pseudomonas* sp. Irchel 3A7, and *Pseudomonas* sp. REP124A.
415 Furthermore, we identified two distinct lineages of previously unrecognized *Pseudomonas*
416 spp., representing putative novel species associated with blotch symptoms. The strains
417 SM391, SM393, and SM396 formed one group, while the strains SM390, SM397, SM404,
418 SM409, and SM431 formed another, each constituting well-supported, genomically
419 coherent clades according to ANI, dDDH and MLSA.

420 Accurate species identification is essential for understanding pathogen diversity and
421 informing disease management strategies. To resolve the taxonomy of the *Pseudomonas*
422 isolates recovered in this study, we applied multiple complementary approaches, including
423 TYGS, GTDB-TK, ANI, and MLSA. Together, these methods provided a robust
424 framework for evaluating genomic relatedness and enabled high-confidence species
425 assignments. Using this integrative strategy, we clearly resolved several blotch-associated
426 taxa, including *Pseudomonas* "gingeri", *P. tolaasii*, *P.* "*reactans*", *P. yamanorum*, *P.*
427 *agarici*, *P. azotoformans*, *P. pergaminensis*, *P. monsensis*, and *P. simiae*, effectively
428 distinguishing our isolates from their closest type strains. However, some groups required
429 more nuanced interpretation. For example, MLSA clustered isolates SM400 and SM426
430 near *P. allokribbensis* IzPS23^{T} and *P. azerbaijanoccidentalis* SWRI74^{T}, yet ANI and

431 GTDB-TK-based dDDH values demonstrated clear genomic distinctiveness, supporting
432 their classification as independent species. Likewise, isolate SM447 showed <70% dDDH
433 similarity to *P. tensinigenes* based on TYGS; however, ANI-based inference provided
434 improved resolution at the species level. A subset of four isolates (SM412, SM422, SM425,
435 SM440) was identified as *Pseudomonas* sp. NC02 according to GTDB-TK. Due to
436 insufficient genome quality for these reference taxa, they could not be fully evaluated using
437 FastANI or MLSA methods. Therefore, we applied GGDC, which confirmed that all four
438 isolates belong to the *Pseudomonas* sp. NC02 lineage. Similarly, SM430 and SM415
439 identified to be *Pseudomonas* sp. REP124 and *Pseudomonas* sp. Irchel 3A7, respectively.
440 Together, these results highlighted the necessity of multi-method taxonomic frameworks
441 when describing *Pseudomonas* diversity in the mushroom environment. BOX-PCR
442 fingerprinting proved valuable as an initial screening tool to capture genomic diversity
443 across all 76 blotch-associated isolates. Although BOX-PCR revealed substantial
444 heterogeneity, its clustering patterns did not correspond with ANI or MLSA-based
445 phylogenies, reflecting differences in repetitive element dynamics rather than true
446 evolutionary relationships. As seen in other bacterial genera such as *Streptomyces*, BOX-
447 PCR is well-suited for rapid delineation of non-redundant isolates but offers limited
448 resolution for deeper taxonomic or phylogenetic inference (20–22). Accordingly, in this
449 study, it served primarily as a high-throughput preselection method prior to whole-genome
450 analyses.
451 Among the novel blotch-associated taxa identified in this study, *Pseudomonas*
452 *azotoformans* was particularly abundant, representing a notable expansion of the known
453 ecological range of this species. *P. azotoformans* has primarily described in plant-
454 associated contexts, most notably as a pathogen of cereal crops such as rice (23), and as an
455 antagonist of several important plant pathogens, including *Fusarium fujikuroi* (24),
456 *Colletotrichum* spp. (25), *Pseudomonas syringae* pv. *actinidiae* (26), and *Alternaria*
457 *brassicae* (27). This host expansion may be facilitated by the species' exceptional tolerance
458 to a wide range of abiotic stresses, including heavy metals, salinity, drought, antibiotics,
459 and extreme temperatures, traits that likely enhance persistence in managed agricultural
460 environments. In support of its ecological versatility, *P. azotoformans* has also been

461 implicated in the blue discoloration of rabbit carcasses (28) and detected in food-processing
462 environments (29). Collectively, these observations indicate that *P. azotoformans* is a
463 highly adaptable generalist capable of colonizing diverse hosts and niches, raising
464 important questions about its evolutionary trajectory, transmission pathways, and potential
465 role in emerging disease complexes across agricultural and food systems. Its prevalence in
466 mushroom blotch is likely facilitated by its capacity to persist in acidic substrates such as
467 peat moss, the primary component of mushroom casing soil. Although commercial casing
468 is adjusted to a higher pH, *P. azotoformans* may remain favored due to its inherent acid
469 tolerance and resilience to pasteurization, enabling survival and subsequent proliferation
470 within the mushroom production environment. In addition to *P. azotoformans*, we also
471 reported the first association of *P. pergaminensis* with mushroom blotch. This species was
472 originally isolated from the wheat rhizosphere during tillering (30) and is used as a bio-
473 stimulant to enhance crop performance. While not previously linked to mushroom
474 pathogenesis, *P. pergaminensis* possesses genomic traits consistent with rhizosphere
475 competence, including phosphate and zinc solubilization and the secretion of extracellular
476 lytic enzymes such as phospholipases and proteases (30, 31) which may similarly facilitate
477 colonization and symptom development on mushroom tissues.
478 The mechanisms underlying discoloration and pitting caused by *Pseudomonas* species
479 remain poorly understood. However, accumulating evidence suggests that extracellular
480 metabolites, such as cyclic lipopeptides (tolaasin), siderophores, degradative enzymes
481 (proteases and lipases), and volatiles (tovsins, DMDS), play central roles in tissue
482 degradation and corrosion processes (3, 32). These compounds mediate microbial
483 competition, surface colonization, and host-pathogen interactions, all of which may
484 contribute to blotch-like symptoms on mushroom caps. To explore this biochemical basis,
485 we employed antiSMASH to predict the families of secondary metabolites encoded by all
486 isolates and to assess their diversity and distribution. Heterogeneity in BGCs was evident
487 across isolates, encompassing CLPs, siderophores, antibiotics, and volatile compounds.
488 CLPs represent a major class of multifunctional secondary metabolites predominantly
489 produced by *Pseudomonas* spp. Among the CLPs, WLIP has been identified as a diagnostic
490 marker for the interaction between tolaasin and the cyclic WLIP produced by *Pseudomonas*

491 *"reactans"* (33), which manifests as a dense white line when the two strains are grown
492 adjacently on agar. The white line reaction is highly structure-specific; WLIP analogues
493 such as viscosin, containing L-Leu instead of D-Leu at position 5, and viscosinamide, a
494 viscosin variant with D-Gln replacing D-Glu at position 2, fail to induce a white line in the
495 presence of *P. tolaasii* (33, 34), highlighting the strict molecular complementarity between
496 WLIP and tolaasin. However, accumulating evidence indicates that this interaction is not
497 exclusive. CLPs other than WLIP, including orfamides A, viscosin, and massetolide A, can
498 also form visible white lines with tolaasin (18). Similarly, sessilins, which are structurally
499 related to tolaasin, induce white line formation through co-precipitation with orfamides
500 (35). Further evidence suggests that WLIP secretion is not restricted to *P. reactans*; *P.*
501 *fluorescens* and *P. putida* strains also produce WLIP (36). In the present study, we observed
502 similar results related to WLIP. *Pseudomonas pergaminensis*, which produces viscosin and
503 orfamides B but no detectable WLIP, formed a clear white line with *P. tolaasii* BP1106.
504 *P. azotoformans*, despite limited CLP production, also induced a white line. Notably, *P.*
505 *aeruginosa* LMG 1272, which lacks canonical CLP biosynthetic genes associated with
506 WLR, nonetheless forms a precipitate when co-cultured with *P. tolaasii* (37). Additionally,
507 *Pseudomonas* species cluster 2 isolates (SM391, SM393, and SM396), which are positive
508 for viscosin production, produced detectable white lines when confronted with *P. tolaasii*
509 BP1106. These observations suggest that WLR formation is not strictly dependent on a
510 single WLIP-tolaasin pair. Rather, variations in peptide stereochemistry, fatty acid chain
511 length, or CLP production levels may influence diffusion and co-precipitation dynamics,
512 resulting in differences in white line intensity and morphology. Siderophore BGCs,
513 including EDHA, yersiniabactin, Ni-siderophore, enantio-pyochelin, and azotobactin D,
514 were distributed among the isolates, consistent with the central role of iron acquisition in
515 bacterial fitness (38-40). However, the canonical siderophore pyoverdine, commonly
516 associated with fluorescent *Pseudomonas* species, was not detected at sufficient similarity
517 levels in any of the genomes. Furthermore, although tolaasin-like clusters were detected
518 with moderate similarity (50–75%) in *P. pergaminensis*, *P. yamanorum*, and species cluster
519 3, white-line agar assays confirmed the absence of tolaasin activity. Together, these results
520 indicate that some isolates harbor highly divergent or nonfunctional tolaasin-like loci,

521 highlighting the limitations of BGC-based predictions and the need for more detailed
522 domain-level annotation, proteomic analyses, and chemical validation to accurately
523 determine metabolite production.
524
525 Comparative pangenome analysis of *Pseudomonas tolaasii*, *P. pergaminensis*, *P.* "*gingeri*"
526 and *P. azotoformans* revealed that only *P. azotoformans* possessed a significantly larger
527 accessory genome relative to its core genome. This expanded accessory fraction
528 corresponds with its broad ecological distribution, siderophore production, and
529 environmental tolerance, reflecting high genomic plasticity for rapid adaptation. To assess
530 genome diversity trends, we modeled core and pangenome trajectories using Tettelin's
531 power-law regression, Core genome: $Yc = Ae^{(-Bx)} + C$; Pangenome: $Yp = Ax^B + C$,
532 where γ (exponent B) indicates openness (γ > 0 = open; γ < 0 = closed) (41). Estimated γ
533 values were 0.049 (*P. tolaasii*), 0.056 (*P. pergaminensis*), 0.046 (*P. "gingeri"*), and 0.085
534 (*P. azotoformans*). While all species suggest theoretically open pangenomes, the values
535 approach the threshold for closure, and limited genome sampling constrains prediction
536 accuracy. Existing literature similarly reports an open pangenome for *P. tolaasii* (42) but
537 broader taxonomic data remain scarce.
538 The findings presented here enhance the current understanding of blotch disease etiology,
539 revealing a greater taxonomic and functional diversity among the pathogens than
540 previously recognized, and extending global insights into the complex bacterial community
541 responsible for mushroom blotch. To our knowledge, this study provides the first evidence
542 that *P. azotoformans*, *P. pergaminensis*, *P. monsensis*, *P. tensinigenes*, and *P. simiae* cause
543 blotch in *Agaricus bisporus*, overturning the long-held assumption that the disease is
544 primarily driven by *P. tolaasii* and *P. "gingeri"*. Species identities were robustly resolved
545 through ANI, TYGS, GTDB-TK, GGDC, and MLSA. Genome comparisons revealed
546 substantial diversity among pathogens, with *P. azotoformans* showing pronounced
547 genomic expansion indicative of broad ecological adaptability. Secondary metabolite
548 profiling and white-line assays further uncovered molecular features likely contributing to
549 virulence and competitive fitness. Together, these findings provide the most
550 comprehensive genomic and phenotypic characterization of blotch-associated

551 *Pseudomonas* to date, demonstrating that blotch is a multispecies disease. As newly
552 emerging pathogens become increasingly prevalent, strain-level diagnostics and genomic
553 surveillance will be critical for early detection and improved disease management in
554 commercial mushroom production.
555

556 **MATERIAL AND METHODS**

557 **Isolation of *Pseudomonas* spp. from white button mushrooms**

558 White button mushrooms displaying bacterial blotch symptoms were collected between
559 April and May 2025 from two major commercial mushroom farms in the southern part of
560 the United States, hereafter referred to as Farm X and Farm Y. Farm X produces
561 approximately 28 million pounds of white button mushrooms annually, while Farm Y
562 produces about 30 million pounds per year. Samples were collected from two separate
563 production rooms at each farm. At Farm X, sampling was conducted during the second and
564 third flushes, while at Farm Y, it occurred during the first flush. At the time of collection,
565 the observed disease incidence was significantly higher at Farm X (30%) compared to Farm
566 Y (1-2%). Symptomatic mushrooms were transported to the laboratory under cold
567 conditions in individual ziplock bags, and bacterial isolation was conducted within 24 to
568 48 h of arrival. Upon arrival, the mushrooms were gently rinsed with sterile distilled water
569 to remove surface debris. Approximately 1 cm^2 of tissue was excised from the margin
570 between diseased and healthy areas using a sterile scalpel. Each tissue sample was
571 transferred into a microcentrifuge tube containing 1 mL of 10% sodium hypochlorite
572 (NaOCl), vortexed for 2 s, and allowed to stand at room temperature for 30 s for surface
573 disinfection. The samples were subsequently rinsed twice with 1 mL of sterile distilled
574 water, briefly vortexing after each rinse. The disinfected tissue was then macerated in 100
575 µL of 0.01 M sterile phosphate buffer (pH 7.0) using a sterile disposable pestle, and the
576 homogenate was vortexed to ensure a uniform suspension. Serial dilutions were prepared,
577 and a 10 µL aliquot from each dilution was streaked onto King's B (KB) (43) agar plates,
578 supplemented with novobiocin (45 µg mL^{-1}), penicillin (75 units mL^{-1}), and cycloheximide
579 (75 µg mL^{-1}) (44). As a control, isolation was also performed from one asymptomatic
580 mushroom collected at each site. All plates were incubated at 27°C for 48 h to allow for

581 bacterial growth. Morphologically distinct bacterial colonies were re-streaked onto freshly
582 prepared KB plates until pure single-colony isolates were obtained. Pure cultures were
583 preserved in 50% glycerol at -80°C for subsequent analyses.
584
585 **Genomic fingerprinting of bacterial isolates**
586 A total of 76 bacterial isolates were selected for BOX-PCR fingerprinting to assess genetic
587 diversity and identify representative isolates for subsequent analyses. A single colony from
588 each isolate was suspended in 50 µL of sterile distilled water, heated at 95°C for 10 min to
589 lyse the cells, immediately chilled on ice for 2 min, and centrifuged at 12,000 × g for 5 min
590 to pellet cell debris. One microliter of the supernatant was used directly as the DNA
591 template for BOX-PCR amplification using the BOXA1R primer (5′-
592 CTACGGCAAGGCGACGCTGACG-3′), following a modified protocol by Rademaker et
593 al. (1998) (21). The PCR reaction mixture contained 1× Green GoTaq buffer,
594 0.08 mg mL^{-1} BSA (NEB), 10% DMSO, 1.25 mM dNTPs, 1.76 µM BOXA1R primer, 1.25
595 U GoTaq G2 DNA polymerase (Promega), and 1 µL of DNA template, for a total volume
596 of 25 µL. PCR amplification was performed in an Applied Biosystems Veriti 96-well
597 thermal cycler with the following cycling conditions: initial denaturation at 95°C for 2 min;
598 29 cycles of 94°C for 3 s, 92°C for 30 s, 50°C for 1 min, and 65°C for 8 min; followed by
599 a final extension at 65°C for 8 min. Amplified products were separated by electrophoresis
600 on 1.5% (w/v) molecular-grade agarose gels in 0.5× TAE buffer (Quality Biological) at 60
601 V and 30 mA for 16 h at 4°C. The gels were visualized, and banding patterns were captured
602 using the Biorad gel doc XR imaging system. DNA fingerprint profiles were further
603 analyzed using ImageJ (45) for pattern recognition and assessment. Pairwise dissimilarities
604 among isolates were calculated using Jaccard's distance (46), and hierarchical clustering
605 was performed with the unweighted pair group method with arithmetic mean (UPGMA)
606 (47) using R software (v4.4.1). Clusters were defined at a 90% similarity threshold, and a
607 binary heatmap was generated to visualize variation in band distribution among isolates.
608
609
610

611 **Pathogenicity Assay**

612 Based on the genetic dissimilarity analysis, 61 isolates were selected for *in vitro*
613 pathogenicity testing. Bacterial suspensions for inoculation were prepared from 5 mL
614 overnight cultures grown in KB broth at 27°C with shaking at 120 rpm for 24 h. The
615 cultures were centrifuged at 8,000 rpm for 10 min, and the resulting cell pellets were
616 washed once with 0.01 mM phosphate-buffered saline (PBS), followed by centrifugation.
617 The cells were resuspended in the same buffer, and the optical density at 600 nm (OD_{600})
618 was adjusted to 0.5 using a Bio-Rad SmartSpec™ 3000 spectrophotometer, corresponding
619 to approximately 10^9 colony-forming units (CFU) per mL. *Pseudomonas protegens*
620 BP1304 and *Pseudomonas tolaasii* BP1106 were used as negative and positive controls,
621 respectively. Pathogenicity assays were performed on fresh, healthy white button
622 mushrooms obtained from a local market. To maintain high humidity, sterile plastic trays
623 were lined with moist filter paper. The mushroom caps were surface sterilized by
624 immersion in 10% sodium hypochlorite (NaOCl) for 30 s, rinsed twice with sterile distilled
625 water, and air-dried under sterile conditions. The stalks were removed, and the epidermal
626 layer of the cap surface was peeled away to expose the inner tissue. Caps were then cut
627 into uniform cubes (4 cm × 2 cm) using sterile scalpels, and each cube was placed
628 individually in a sterile petri dish to prevent cross-contamination. Three inoculation sites
629 were designated on each cube using a sterile No. 4 cork borer (4 mm diameter) to mark
630 circular areas, following Henkels et al. (2014) (18). A 10 µL aliquot of bacterial suspension
631 was applied to each marked site. For each isolate, nine replicate mushroom cubes were
632 tested, and the entire assay was independently repeated three times. Petri dishes containing
633 the mushroom cubes were sealed and incubated in the dark at 27°C for three days.
634 Symptom development was monitored and photographed daily to assess tissue maceration,
635 pitting, or discoloration until 72 h. Severity scores were assigned as follows: 1= mild or
636 slow discoloration; 2= rapid tissue discoloration without tissue pitting; 3= extensive
637 discoloration accompanied by tissue pitting.

638

639

640

641 **Florescence and White Line Agar (WLA) test**

642 All isolates (*n* = 61) were cultured on KB medium, and their ability to produce fluorescent
643 pyoverdine and related metabolites was evaluated under UV light (365 nm) after 48 h of
644 incubation. The white line reaction assay was performed to assess the production of
645 extracellular lipopeptides, including tolaasin and WLIP (white line inducing principle),
646 following the methods described by Osdaghi et al. (2019) (2). Briefly, *P. fluorescens* Pf-
647 5P was streaked against each isolate to evaluate tolaasin production, while *Pseudomonas*
648 *tolaasii* BP1106 was used to assess the secretion of WLIP and related lipopeptides. On
649 King's B agar, two loopfuls of each test isolate were streaked approximately 8 mm from
650 the reference strain. Plates were incubated at 27 °C, and white-line formation was
651 monitored over a 72 h period. A positive white-line reaction was defined as the formation
652 of a distinct white precipitate at the interface between the test isolate and either
653 *Pseudomonas fluorescens* Pf-5P or *P. tolaasii* BP1106.

654

655 **DNA extraction and Whole Genome Sequencing (WGS)**

656 Genomic DNA from the (*n* = 61) isolates was extracted using the Quick-DNA Fecal/Soil
657 Microbe MiniPrep Kit (Zymo Research). The quality and concentration of the DNA were
658 verified using a Bio-Rad Universal Hood Gel Doc XR UV Transilluminator (200 VA)
659 system, and quantity was evaluated using Nanodrop spectrophotometer (Thermo Fisher
660 Scientific). Whole-genome sequencing was performed by SeqCenter (Pittsburgh).
661 Sequencing libraries were constructed using the Illumina DNA Prep Kit (tagmentation-
662 based) with custom IDT 10-bp unique dual indices (UDI) and an average insert size of
663 approximately 280 bp. Paired-end sequencing (2 × 151 bp) was conducted on an Illumina
664 NovaSeq X Plus platform. Raw read demultiplexing, adapter removal, and initial quality
665 control were performed using bcl-convert (v4.2.4).

666

667 **Genome assembly**

668 The quality of the reads was assessed with FastQC (v0.12.1) (48). Based on the quality
669 metrics, low-quality bases and residual adapter sequences were trimmed using Trim Galore
670 (v0.6.10), applying a Phred quality cutoff of 20. To remove potential primer or adapter

contamination, 15 bases were clipped from the 5′ ends and 10 bases from the 3′ ends of both forward and reverse reads. Paired reads that passed all quality filters were retained for downstream analyses. High-quality reads were assembled de novo using SPAdes (v4.0.0) (49), and contigs shorter than 500 bp and a K-mer coverage of less than 2.0 were filtered out. Assembly quality was evaluated with QUAST (v5.2.0) (50), and genome completeness was estimated using BUSCO (v5.8.3) based on lineage-specific single-copy orthologs (51). Only *Pseudomonas* strains (n = 57) were used for downstream analysis. Assembled genomes for all 57 strains were submitted to NCBI under Bio Project PRJNA1377199, with accession numbers SAMN53759319 to SAMN53759375.

Genome-wide comparisons

The identity of each isolate was determined using data from assembled genome sequences submitted to the Type (Strain) Genome Server TYGS, (https://tygs.dsmz.de) for whole-genome-based taxonomic analysis (52, 53). TYGS calculates digital DNA–DNA hybridization (dDDH) values using multiple formulas, including dDDH4, which estimates nucleotide identity within high-scoring genome alignments. A dDDH4 value above 70% is used for taxonomic delineation (53). For further classification, the Average Nucleotide Identity (ANI) based Genome Taxonomy Database classify workflow GTDB-Tk (v2.4.1) (54) was used with a threshold of 95% to determine species boundaries. TYGS and GTDB-Tk were also used to identify the closest relative strains, including type strains, for comparative analysis. Pairwise ANI values of the isolates and their closest relatives were computed using all-versus-all strategies with FastANI (v1.34) (Dataset S02) (55). ANI similarity values greater than 95% were used to construct a phylogenetic heatmap in RStudio using the pheatmap package (v1.0.13). When the above methods were insufficient to confidently resolve species-level identity, we further assessed genomic relatedness using the Genome-to-Genome Distance Calculator (GGDC) (https://ggdc.dsmz.de/ggdc.php) (56).

Multi-locus sequence analysis (MLSA) was performed to infer the evolutionary history of the bacterial genomes using eight conserved housekeeping genes (*rpoD, rpoB, recA, gapA, gltA, atpD, gyrB,* and *ileS*) from nine reference strains (Dataset S02). A total of 31 closely

701 related reference sequences, including *Pseudomonas lurida* LMG21995^T as the outgroup,
702 were retrieved from NCBI and included in the phylogenetic analysis (*Dataset S01*).
703 Reference strains included all available type strains unless otherwise noted. Type strain
704 names were confirmed with The List of Prokaryotic names with Standing in Nomenclature
705 (LPSN) (57). Gene sequences were extracted and aligned using AutoMLSA2 (v2.0.9.0)
706 (https://github.com/davised/automlsa2), which features an automated pipeline that
707 identifies housekeeping genes, performs multiple sequence alignment using MAFFT
708 (v7.520), and concatenates the alignments. The concatenated alignment totaled 176,583
709 bp and was used to generate a maximum-likelihood phylogenetic tree using IQ-TREE
710 (v3.0.1) with node support values based on 1,000 bootstraps (58, 59). The phylogenetic
711 tree was visualized using iTOL (v7.2.2) (60).
712
713 **Core and Pan genome analysis**
714 Pan-genome analysis was performed on all 57 *Pseudomonas* isolates, without
715 incorporating external NCBI reference genomes. Additionally, for the four most abundant
716 species *P. tolaasii*, *P. gingeri*, *P. azotoformans*, and *P. pergaminensis* pan-genome and
717 core-genome profiles were constructed by integrating corresponding NCBI reference
718 genomes. All the NCBI reference accessions are listed in Dataset S02. Gene prediction and
719 functional annotation were performed with Prokka v1.14.6 (61) with default parameters.
720 The resulting GFF files were used for the pan-genome analysis with Roary v3.13.0 (62),
721 applying a minimum BLASTp identity of 90% for both species cluster analyses and for all
722 strains. For each species group, maximum-likelihood phylogenetic analysis was conducted
723 using RAxML v8.2.10 based on the concatenated core-gene alignments generated by
724 Roary. This analysis employed the GTR+GAMMA substitution model with rapid bootstrap
725 searches, with 100 bootstrap replicates to identify the best-scoring tree (63). Phylogenetic
726 trees were visualized and annotated in iTOL (v7.2.2). Both the resulting tree and gene
727 presence/absence matrices were explored and visualized using Phandango (64).
728
729
730

731

732 **Secondary metabolite prediction**

733 Secondary metabolite biosynthetic gene clusters (BGCs) were identified using antiSMASH
734 v7.0.0 (65) with default parameters. To focus on conserved clusters, only BGCs with over
735 30% sequence similarity were retained for further analysis. The resulting BGC profiles
736 were compiled for all isolates, and the presence or absence of each predicted cluster type
737 was visualized in R (v4.4.1) using ggplot2 to compare secondary metabolite cluster
738 distributions among the species groups.

739

740 **ACKNOWLEDGMENTS**

741

742 This work was supported by the USDA SCRI: PENW-2023-05649 and by the Research
743 Capacity Fund (Hatch) program, project award no. 7010682, from the U.S. Department of
744 Agriculture's National Institute of Food and Agriculture. The authors also acknowledge
745 Dr. Fabiano Perina for the assistance with the rep-PCR assay and Dr. Carolee Bull who
746 kindly shared the bacterial strains BP1304 and BP1106 used in this study.

747

748 **REFERENCES**

749 1. D. J. Royse, J. Baars, Q. Tan, "Current overview of mushroom production in the world"
750 in *Edible and Medicinal Mushrooms: Technology and Applications*, D. C. Zied, A.
751 Pardo-Giménez, Eds. (Wiley-Blackwell, 2017), pp. 5–13.
752 2. E. Osdaghi, *et al*., 100 years since Tolaas: Bacterial blotch of mushrooms in the 21st
753 century. *Plant Dis.* 103, 2714–2725 (2019).
754 3. C. Soler-Rivas, S. Jolivet, N. Arpin, J. M. Olivier, H. J. Wichers, Biochemical and
755 physiological aspects of brown blotch disease of *Agaricus bisporus*. *FEMS Microbiol.*
756 *Rev.* 23, 591–614 (1999).
757 4. G. Eger, Experiments and comments on the action of bacteria on sporophore initiation
758 in *Agaricus bisporus*. *Mushroom Sci.* 8, 719–725 (1972).
759 5. T. Fermor, et al., Microbiological properties of casing. *Mushroom Sci.* 15, 447–454
760 (2000).
761 6. W. C. Wong, P. T. Fletcher, Identification of *Pseudomonas tolaasii*: The white line in
762 agar and mushroom tissue block rapid pitting tests. *J. Appl. Bacteriol.* 47, 401–407
763 (1979).
764 7. M. Fatmi *et al*., "*Pseudomonas syringae* pathovars and related pathogens:
765 Identification, epidemiology and genomics" in *Pseudomonas syringae Pathovars and*

766 *Related Pathogens*, M. Fatmi, A. Collmer, N. S. Iacobellis, J. Mansfield, J. Murillo, N.
767 W. Schaad, Eds. (Springer, 2008).
768 8. F. P. Geels, L. P. W. Hesen, L. J. L. D. van Griensven, Brown discolouration of
769 mushrooms caused by *Pseudomonas agarici*. *J. Phytopathol.* 140, 249–259 (1994).
770 9. J. M. Young, Drippy gill: A bacterial disease of cultivated mushrooms caused by
771 *Pseudomonas agarici* sp. nov. *N. Z. J. Agric. Res.* 13, 977–990 (1970).
772 10. J. M. Wells, *et al*., Postharvest discoloration of the cultivated mushroom *Agaricus*
773 *bisporus* caused by *Pseudomonas tolaasii*, *P.* "reactans," and *P.* "gingeri."
774 *Phytopathology* 86, 1098–1104 (1996).
775 11. S.A.C. Godfrey, J.W. Marshall, J.D. Klena, Genetic characterization of *Pseudomonas*
776 'NZI7'-a novel pathogen that results in a brown blotch disease of *Agaricus bisporus*, *J.*
777 *Appl. Microbiol.* 91, 412–420 (2001).
778 12. T. Taparia, et al., Molecular characterization of *Pseudomonas* from *Agaricus bisporus*
779 caps reveals novel blotch pathogens in Western Europe. *BMC Genomics* 21, 1–15
780 (2020).
781 13. P. Munsch, V. A. Geoffroy, T. Alatossava, J. M. Meyer, Application of siderotyping
782 for characterization of *Pseudomonas tolaasii* and "*Pseudomonas reactans*" isolates
783 associated with brown blotch disease of cultivated mushrooms. *Appl. Environ.*
784 *Microbiol.* 66, 4834–4841 (2000).
785 14. Z. Huang, F. Li, H. Li, M. Jiang, B. Liu, First report of *Pseudomonas extremorientalis*
786 causing brown blotch disease of white button mushroom (*Agaricus bisporus*) in China.
787 *Plant Dis.* 109, (2025). https://doi.org/10.1094/PDIS-06-25-1178-PDN
788 15. M. Hamidizade, *et al*., Bacterial brown pit, a new disease of edible mushrooms caused
789 by *Mycetocola* sp. *Plant Dis.* 104, 1445–1454 (2020).
790 16. Z. Huang, Y. Huang, Y. Nie, B. Liu, Biological characteristics of two pathogens
791 causing brown blotch in *Agaricus bisporus* and toxin identification of *Cedecea neteri*.
792 *Phytopathol. Res.* 6, 1–12 (2024).
793 17. K. Morihara, J. Y. Homma, "Bacterial enzymes and virulence" in *Bacterial Enzymes*
794 *and Virulence*, I. A. Holder, Ed. (CRC Press, Boca Raton, FL, 1985), pp. 41–79.
795 18. M. D. Henkels, *et al*., *Pseudomonas protegens* Pf-5 causes discoloration and pitting of
796 mushroom caps due to antifungal metabolites. *Mol. Plant-Microbe Interact.* 27, 733–
797 746 (2014).
798 19. M. Gomila, A. Peña, M. Mulet, J. Lalucat, E. García-Valdés, Phylogenomics and
799 systematics in *Pseudomonas*. *Front. Microbiol.* 6, 214 (2015).
800 20. L. M. Bilung, *et al*., Presence of *Bacillus cereus* from local unhusked (rough) rice
801 samples in Sarawak, Malaysia. *J. Sustain. Sci. Manag.* 13, 181–187 (2018).
802 21. J. L. W. Rademaker, F. J. Louws, F. J. de Bruijn, "Characterization of the diversity of
803 ecologically important microbes by rep-PCR genomic fingerprinting" in *Molecular*

Microbial Ecology Manual, J. D. Van Elsas, et al., Eds. (Kluwer Academic Publishers, Dordrecht, The Netherlands, 1998).

22. A. van Belkum, M. Sluijuter, R. de Groot, H. Verbrugh, P. W. Hermans, Novel BOX repeat PCR assay for high-resolution typing of *Streptococcus pneumoniae* strains. *J. Clin. Microbiol*. 34, 1176-1179 (1996).
23. H. Iizuka, K. Komagata New species of *Pseudomonas* belonging to the fluorescent group (Studies on the microorganisms of cereal grains. Part V). *J Agric Chem Soc Jpn* 37:137-141(1963).
24. P. Wiemann, *et al*., Deciphering the cryptic genome: Genome-wide analyses of the rice pathogen *Fusarium fujikuroi* reveal complex regulation of secondary metabolism and novel metabolites. *PLoS Pathog.* 9, e1003475 (2013).
25. I. Popescu, A. K. Loganathan, H. R. Graham, and T. J. Avis, Antifungal activity of *Bacillus velezensis* and *Pseudomonas azotoformans* isolated from compost tea against anthracnose (*Colletotrichum* spp.) on strawberry fruit. *Plant Pathol.* 73, 2419-2428 (2024).
26. C. Correia, *et al*., *Pseudomonas azotoformans* and *Pseudomonas putida*: Novel kiwifruit-native biological control agents against *Pseudomonas syringae* pv. *actinidiae*. *Biol. Control* 201, 105706 (2025).
27. A. Bhattacharya, P. Verma, C. Bharti, and N. K. Arora, Characterization of antifungal metabolites produced by plant growth promoting bacterial endophyte *Pseudomonas azotoformans* SS7 from *Brassica juncea* as a biocontrol tool for *Alternaria brassicae*. *Arch. Phytopathol. Plant Prot.* 58, 604-629 (2025).
28. E. Circella, *et al*., *Pseudomonas fluorescens* group bacteria responsible for chromatic alteration on rabbit carcasses. *Ital. J. Food Saf.* 11, 10042 (2022).
29. G. M. B. Thomassen, T. Reiche, C. E. Tennfjord, L. Mehli, Antibiotic resistance among *Pseudomonas* in salmon processing environments. *Microorganisms* 10, 1401 (2022).
30. M. Díaz, *et al*., Agronomic efficiency and genome mining analysis of the wheat-biostimulant rhizospheric bacterium *Pseudomonas pergaminensis* sp. nov. strain 1008T. Front. *Plant Sci*. 13, 894985 (2022).
31. Q. Xiang, W. Dong, X. Zheng, X. Sheng, Integrated physiological and metabolomic analysis reveals the cytochrome oxidase gene ccoQ-mediated biotite dissolution by *Pseudomonas pergaminensis* F77. *Chem Geol* 694 (2025).
32. P. Lo Cantore, A. Giorgio, N. S. Iacobellis, Bioactivity of volatile organic compounds produced by *Pseudomonas tolaasii*. *Front Microbiol* 6 (2015).
33. H. Rokni-Zadeh, A. Mangas-Losada, R. de Mot, PCR Detection of Novel Non-ribosomal Peptide Synthetase Genes in Lipopeptide-Producing *Pseudomonas*. *Microb Ecol* 62, 941–947 (2011).
34. H. Rokni-Zadeh, W. Li, E. Yilma, A. Sanchez-Rodriguez, R. De Mot, Distinct lipopeptide production systems for WLIP (white line-inducing principle) in

Pseudomonas fluorescens and *Pseudomonas putida*. *Environ Microbiol Rep* 5, 160–169 (2013).

35. J. D'aes, *et al.*, To settle or to move? The interplay between two classes of cyclic lipopeptides in the biocontrol strain *Pseudomonas* CMR12a. *Environ Microbiol* 16, 2282–2300 (2014).
36. H. Rokni-Zadeh, *et al.*, Genetic and functional characterization of cyclic lipopeptide white-line-inducing principle (WLIP) production by rice rhizosphere isolate pseudomonas putida RW10S2. *Appl Environ Microbiol* 78, 4826–4834 (2012).
37. F. Salari, *et al.*, Draft Genome Sequence of *Pseudomonas* aeruginosa Strain LMG 1272, an Atypical White Line Reaction Producer. *Microbiol Resour Announc* 9, 01363-19 (2020).
38. M. G. P. Page, Siderophore conjugates. *Ann N Y Acad Sci* 1277, 115–126 (2013).
39. R. Saha, N. Saha, R. S. Donofrio, L. L. Bestervelt, Microbial siderophores: A mini review. *J Basic Microbiol* 53, 303–317 (2013).
40. P. N. Jimenez, *et al.*, Role of PvdQ in *Pseudomonas aeruginosa* virulence under iron-limiting conditions. *Microbiology* (*Reading*) 156, 49–59 (2010).
41. H. Tettelin, D. Riley, C. Cattuto, D. Medini, Comparative genomics: the bacterial pan-genome. *Curr Opin Microbiol* 11, 472-477 (2008).
42. Z. Liu, *et al.*, Characterization, Pathogenicity, Phylogeny, and Comparative Genomic Analysis of *Pseudomonas tolaasii* Strains Isolated from Various Mushrooms in China. *Phytopathology* 112, 521–534 (2022).
43. E. O. King, M. K. Ward, D. E. Raney, Two simple media for the demonstration of pyocyanin and fluorescin. *J. Lab. Clin. Med.* 44, 301–307 (1954).
44. K. Suyama, H. Negishi, S. Wakimoto, Selective medium for isolation of *Pseudomonas tolaasii*, the causal agent of bacterial blotch of cultivated mushrooms. *J. Agric. Sci.* 44, 295–301 (2000).
45. E. A. Sánchez-Jaramillo, L. E. Gasca-Lozano, J. M. Vera-Cruz, L. D. Hernández-Ortega, A. M. Salazar-Montes, Automated computer-assisted image analysis for the fast quantification of kidney fibrosis. *Biology (Basel)* 11, 1227 (2022).
46. P. Jaccard, Nouvelles recherches sur la distribution florale. *Bull. Soc. Vaud. Sci. Nat.* 44, 223–270 (1908).
47. R. R. Sokal, P. H. A. Sneath, *Principles of Numerical Taxonomy* (W. H. Freeman, 1963).
48. S. Chen, Y. Zhou, Y. Chen, J. Gu, fastp: An ultra-fast all-in-one FASTQ preprocessor. *Bioinformatics* 34, i884–i890 (2018).
49. A. Bankevich, et al., SPAdes: A new genome assembly algorithm and its applications to single-cell sequencing. *J. Comput. Biol.* 19, 455–477 (2012).
50. A. Gurevich, V. Saveliev, N. Vyahhi, G. Tesler, QUAST: Quality assessment tool for genome assemblies. *Bioinformatics* 29, 1072–1075 (2013).

882 51. F. A. Simão, R. M. Waterhouse, P. Ioannidis, E. V. Kriventseva, E. M. Zdobnov,
883 BUSCO: Assessing genome assembly and annotation completeness. *Bioinformatics* 31,
884 3210–3212 (2015).
885 52. J. P. Meier-Kolthoff, M. Göker, TYGS is an automated high-throughput platform for
886 genome-based taxonomy. *Nat. Commun.* 10, 2182 (2019).
887 53. J.P. Meier-Kolthoff, A.F. Auch, H.P. Klenk, M. Göker, Genome sequence–based
888 species delimitation with confidence intervals and improved distance functions. *BMC*
889 *Bioinformatics* 14, 60 (2013).
890 54. P. A. Chaumeil, A. J. Mussig, P. Hugenholtz, D. H. Parks, GTDB-Tk v2: Classification
891 with the genome taxonomy database. *Bioinformatics* 38, 5315–5316 (2022).
892 55. C. Jain, L. M. Rodriguez-R, A. M. Phillippy, K. T. Konstantinidis, S. Aluru, High-
893 throughput ANI analysis reveals clear species boundaries. *Nat. Commun.* 9, 5114
894 (2018).
895 56. J.P. Meier-Kolthoff, J.S. Carbasse, R.L. Peinado-Olarte, M. Göker, TYGS and LPSN:
896 a database tandem for fast and reliable genome-based classification and nomenclature
897 of prokaryotes. *Nucleic Acids Res*. 50, D801–D807 (2022).
898 57. A.C. Parte, J. Sardà Carbasse, J.P. Meier-Kolthoff, L.C. Reimer, M. Göker, List of
899 Prokaryotic names with Standing in Nomenclature (LPSN) moves to the DSMZ. *Int J*
900 *Syst Evol Microbiol* 70, 5607–5612 (2020).
901 58. T. Wong, *et al*. "IQ-TREE 3: Phylogenomic Inference Software using Complex
902 Evolutionary Models. [Preprint] (2025) https://doi.org/10.32942/X2P62N (accessed 16
903 December 2025).
904 59. B. Q. Minh, H. A. Schmidt, O. Chernomor, D. Schrempf, M. D. Woodhams, A. von
905 Haeseler, R. Lanfear, IQ-TREE 2: New models and efficient methods for phylogenetic
906 inference in the genomic era. *Mol. Biol. Evol*. 37, 1530–1534 (2020).
907 60. I. Letunic, P. Bork, Interactive Tree of Life (iTOL) v6. *Nucleic Acids Res.* 52, W78–
908 W82 (2024).
909 61. T. Seemann, Prokka: Rapid prokaryotic genome annotation. *Bioinformatics* 30, 2068-
910 2069 (2014).
911 62. A. J. Page, *et al*., Roary: Rapid large-scale prokaryote pan-genome analysis.
912 *Bioinformatics* 31, 3691-3693 (2015).
913 63. M. Stamatakis, RAxML version 8: A tool for phylogenetic analysis and post-analysis
914 of large phylogenies. *Bioinformatics* 30, 1312-1313 (2014).
915 64. J. Hadfield, N. J. Croucher, R. J. Goater, K. Abudahab, D. M. Aanensen, S. R. Harris,
916 Phandango: An interactive viewer for bacterial population genomics. *Bioinformatics*
917 34, 292-293 (2018).
918 65. K. Blin, *et al*., antiSMASH 7.0. *Nucleic Acids Res.* 51, W46-W50 (2023).

919

SI Appendix

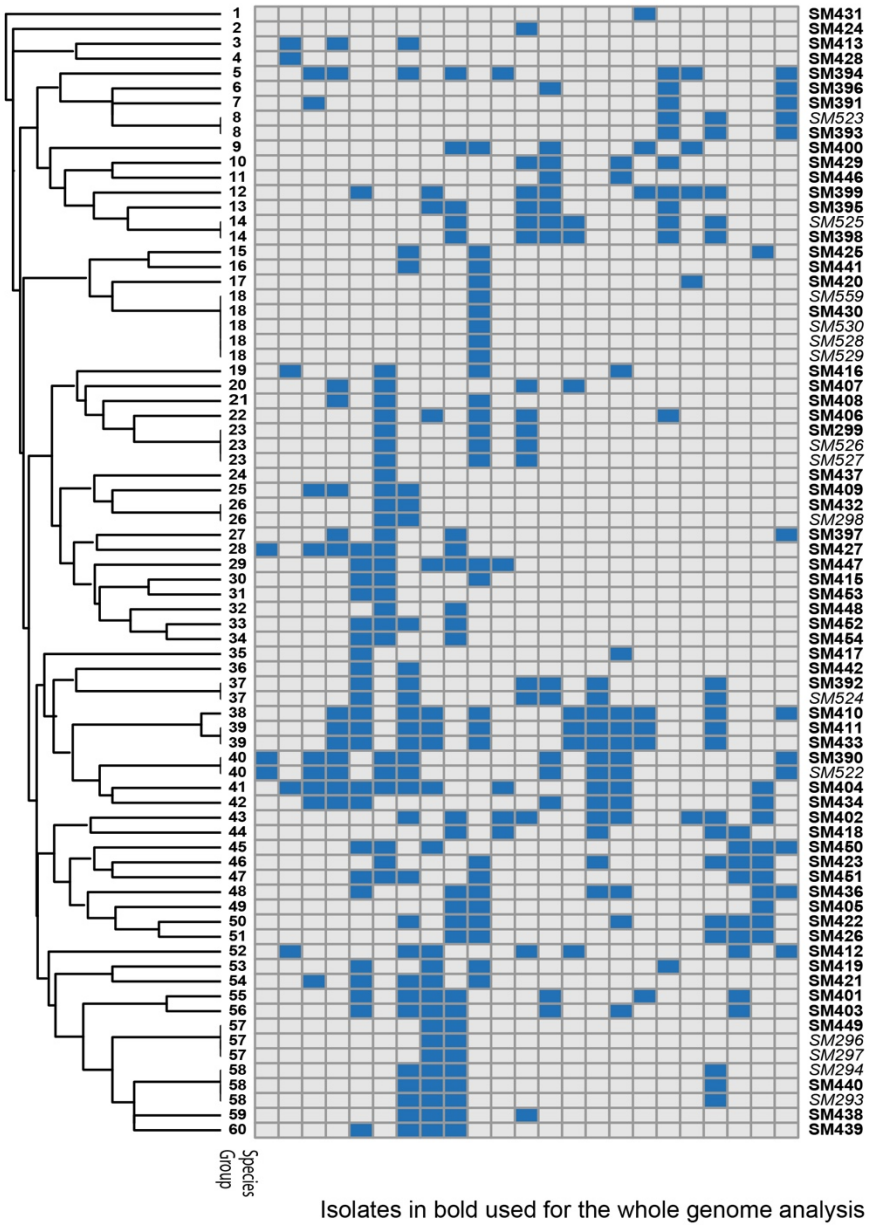

Supplementary Figure 1. ***Genetic diversity of Pseudomonas isolates based on BOX-PCR profiles.*** *BOX-PCR fingerprinting of 77 bacterial isolates produced reproducible banding patterns on agarose gel. A binary data matrix, constructed from the presence or absence of 23 distinct BOX-PCR bands, was used for clustering analysis. The resulting dendrogram revealed 60 clusters at a 90% similarity threshold. Based on these DNA fingerprinting patterns, 15 strains with identical BOX-PCR profiles were isogenic and excluded from further analyses. Isolates shown in* ***bold*** *were selected for whole-genome sequencing.*